An adaptive level set method for medical image segmentation

M. Droske†, B. Meyer‡, M. Rumpf†, K. Schaller‡

† Institut für Angewandte Mathematik,
‡ Klinik für Neurochirurgie,
Universität Bonn

Abstract. An efficient adaptive multigrid level set method for front propagation purposes in three dimensional medical image processing and segmentation is presented. It is able to deal with non sharp segment boundaries. A flexible, interactive modulation of the front speed depending on various boundary and regularization criteria ensure this goal. Efficiency is due to a graded underlying mesh implicitly defined via error or feature indicating values on the cells of the underlying hexahedral grid. A suitable saturation condition ensures an important regularity condition on the resulting adaptive grid. This simplifies the adaptive fast marching method on the compressed data significantly. As an application the segmentation of glioma is considered. Thus the clinician interactively selects a few parameters describing the speed function and a few seed points referring to a single slice of an MRI data set. Then the automatic process of front propagation generates a family of segments corresponding to the evolution of the front in time, from which the clinician finally selects an appropriate segment covered by the gliom. This selection can be based on a visual evaluation of the propagation on a reference slice using the clinicians expert knowledge. Thus, the overall glioma segmentation turns into an efficient, nearly real time process with intuitive and usefully restricted user interaction.

1 Introduction

Robust and efficient segmentation algorithms on digital images are a challenging research topic of increasing interest especially in the last decade. Front propagation methods based on an implicit representation of the evolving front proved to lead to convincing results for basic segmentation purposes [2, 12, 11, 16, 18]. Unfortunately, they require considerable computing time to solve the underlying partial differential equation especially on highly resolved 3D images. Adaptive grid techniques [14] allow to overcome this drawback usually at the cost of storing large hierarchical grid structures explicitly. Hence,

the processing of large data sets on desktop computers is getting question some. We present an alternative approach. It confines with minimal additional data to be stored to describe an adaptive grid of nice regularity properties. This allows the efficient, nearly real time handling of grids larger than 256^3 by an adaptive front propagation algorithm. Furthermore, flexible criteria for the segment boundary depending on a class of concrete segmentation problems can be coded into the propagation speed of the front. Our method is not considered as fully automatic. Indeed, user input is required in advance to fix a few parameters and to select seed points in the segment under consideration. Finally, the user extracts from a resulting family of segments calculated during the front propagation an appropriate candidate. Here his expert knowledge is required to compare the evolution results with the original image data on a suitable slice through the segment. As an important case study we consider a segmentation problem in brain surgery. In order to construct a reliable modeling for tissue segmentation in the level set context, we need a profound understanding about the delicate anatomical and histological structures. One of the major problems in the surgical treatment of intrinsic tumors of the brain is precise determination of the resection zone. This is due to their infiltrative character, which itself correlates with histological grade. In particular, low grade gliomas (WHO grades I and II) and anaplastic gliomas (WHO grade III) may be well visualized on specific Magnetic Resonance Imaging (MRI) sequences, but intraoperative resection control can be ambiguous with marginal differences in consistency between tumor and the surrounding tissue - sometimes even within the tumor itself. The decision as to resect or not to resect certain areas depends mainly on the intraoperative impression and the experience of the respective neurosurgeon. In eloquent brain regions, however, elaborate resection control determines the functional outcome of the patient in an extreme manner, as only few millimeters can be decisive for the further operative result. Refer to [5, 23, 24] for further details.

For that purpose, image guided frameless neuronavigational devices are being integrated into clinical routine at many neurosurgical centers worldwide. These systems allow for preoperative planning of the procedure typically by segmentation of 2D imaging data for subsequent 3D rendering and precise orientation in space. The respective

intracranial lesions may be encircled manually and colour coded on each image slice - if considered necessary. This information may be retrieved during the procedure and serves for guidance and resection control. This slice-by-slice segmentation, however, is time consuming, complicated and error prone. Currently available automatic segmentation tools, on the other hand, proved inaccurate. The "ideal" brain tumor to test the capability and usefulness of such a computerized tool are gliomas, because of their frequent irregular shape.

We have used WHO grade II and III insular gliomas for that purpose. These tumors may grow to considerable size prior to clinical and radiological diagnosis. At a certain stage they may not only infiltrate the insula itself and the adjacent frontal and temporal opercula (types 3a and 3b), but the adjacent temporal, frontoorbital, paralimibic and limbic structures as well (types 5a and 5b). Thus, it is of utmost importance to follow this complex 3D cytoarchitectonic infiltrative order during surgery, and to avoid transgressing these borders into the sensomotoric pathways within the central lobe and/or the basal ganglia.

2 Review of related work

In computer vision literature various methods dealing with segmentation and feature extraction are discussed. The well known technique of the morphological watershed transform [13] creates a tesselation of the image domain Ω in several small regions by considering the image values as intensity niveaus in a topographical landscape. By simulating rainfall, the domain is grouped in catchment basins, regions in which the water drains from all points to the same local intensity minimum. Naturally this method is very sensitive to small variations of the image magnitude and consequently the number of generated regions is undesirably large. To overcome this problem of identifying exhaustively many segments there have been efforts in recent years to reduce the complexity of the tesselation by region merging based on homogeneity criteria [8] or studying the evolution of the catchment basins in Gaussian scalespace [6]. Such techniques can generate unpredictable results and depend to a large extend on user interaction and the quality of the initial partition. Although

improvements have been made [20], the creation of the watersheds is still computationally demanding.

An entirely different and popular approach to visual shape analysis is related to so called *active contour models* and *snakes* [2, 12, 21, 22]. It is based on a curve respective surface evolution, starting from some initial curve or surface which is propagated to achieve a proper approximation of the segment boundary. Active contour models may incorporate a wide range of driving forces. Many of them are based on minimization of combined energy functionals controlling the fairness of the resulting curve on one hand and the attraction to areas of interest such as object boundaries on the other hand. Weighting parameters have to be carefully chosen to find a good balance between these terms. In early works *explicit snakes* with a standard parametric curve representation were used. The key disadvantage of this method is a topological constraint: the curve can not split to approximate boundaries of not simply connected segments. Such problems have been solved by introducing *implicit snakes* models[2, 12], in which the initial curve is interpreted as the zero level curve of a function $\Phi(t, \cdot) : \Omega \rightarrow \mathbb{R}$. The evolution of these snakes is controlled by a PDE [18]. An external term is considered to include information about the initial image. Although contours are able to split in this formulation there remains the problem that the result of the segmentation relies significantly on a good initialization. Furthermore many models have difficulties in progressing into boundary concavities. Adressing these particular problems a new class of external forces has been proposed by deriving from the original image a *gradient vector flow* field in a variational framework [22]. Sensitivity to initialization has been drastically reduced and contours have a more sensible behaviour in the regions of concavities. Furthermore a general variational framework for Mumford-Shah and Geman type functionals [7, 15] has been introduced [9]. Edge boundaries are represented by a continuous function, yielded by the minimization of an energy functional.

3 Levelset based segmentation

Our aim is the development of a robust and flexible segmentation method on images with non sharp segment boundaries. First, let

us give a mathematical definition of a segment, which incorporates sharp criteria for segment boundaries expressed in terms of a boundary indicating function (cf. Section 1 for hints on such criteria in the literature). Later on we will weaken this definition with respect to a evolving scale of segmentation sets. Given a boundary indicator function $\sigma : \Omega \to \mathbb{R}$ on the image domain Ω and a seed set A we can define a segment $\mathcal{S}(A, \sigma)$ as the connected component of the seed set A where $\sigma(\cdot) \leq 0$ holds. Explicitly, we obtain

$$\mathcal{S}(A, \sigma) := \{ y \in \Omega \,|\, \exists\, C^0 \text{ curve } \gamma : [0, 1] \to \Omega,\ \gamma(0) \in A\ \gamma(1) = y,$$
$$\sigma(\gamma(t)) \leq 0\ \forall\, t \in [0, 1] \}\,.$$

This definition implicitly assumes that a precise definition of the segment boundary can be coded in the sharp indicator criteria $\sigma(\cdot) = 0$ for smooth σ on the boundary. Unfortunately, asking for segmentation of certain tissue types on 2D and 3D medical images there is typically not such a precise knowledge of the boundary criteria and location.

Often the identification of a segments requires a trained and experienced clinician who selects an appropriate segment with boundaries located in a transition region on the image. Thereby, it is reasonable to expect the clinicians visual perception to start with some save set A, which should surely be considered as being inside the final segment, then expanded towards the unknown boundary. The expansion is save and thus probably faster where certain criteria to be inside the segment are surely fulfilled. More careful and slow expansion is considered in areas where the different criteria are only partially fulfilled or a quantitative criteria becomes less significant. Finally, the clinician has to decide then and where the criteria are to week to consider a further expansion of the segment.

This observations motivates our effective semiautomatic procedure:

− At first the clinician selects a set A, e. g. picking some points on a single or on a few image slices.
− Furthermore depending on the class of segment - in our application example glioma in the human brain - the speed of front propagation is modeled based on several suitable criteria. E. g. we take into account the image intensity, the intensity gradient,

the curvature, and previous segmentation results on the expected complement set.

– Based on these parameters the efficient adaptive level set algorithm to be described here propagates the segment boundary outwards, starting with the boundary of the set A. The adaptive codes allows an almost real time performance of this algorithm and enables a flexible adjustment of the selected steering parameters.

– Finally the clinician interactively inspects the generated family of evolved segment sets $\mathcal{S}(A,\sigma)(t)$ and selects a proper time T and a corresponding final segmentation result $S:=\mathcal{S}(A,\sigma)(T)$. Visualizing 3D images image slices simultaneously with the 3D segment sets can be considered as a reference for final decision.

Now, we consider the actual mathematical modeling of this procedure. Let us consider a propagation of the boundary $\partial\mathcal{S}_0$ of the initial set $\mathcal{S}_0:=A$ in direction of the outer normal N with speed F, i. e. we ask for evolution curves in 2D or surfaces in 3D $\partial\mathcal{S}(t)$ - bounding our expanding segments $\mathcal{S}(t)$ - with parametrization $x(t)$ with

$$\frac{\partial}{\partial t}x = F(x)N(x)\,.$$

In case of a velocity F which is guaranteed to stay non–negative during the evolution this problem can be reformulated in terms of the time T at which the front reaches a certain position x (cf. [18]). As segmentation is a process in which the front of the segment always propagates outward, we do not rely on negative values for F. Thus, we ask for a function $T : \Omega \rightarrow \mathbb{R}_0^+; x \mapsto T(x)$ such that the generalized *eikonal equation*

$$\|\nabla T\|_2 F = 1 \qquad T|_{\mathcal{S}_0} = 0 \tag{1}$$

holds. Here $\|\cdot\|_2$ denotes the Euclidian norm. Hence, as the corresponding segment at any time t we obtain

$$\mathcal{S}(t):=\{x \in \Omega \mid T(x) \leq t\}$$

There are in general no global, classical solutions. Therefore we consider generalized viscosity solutions [3] and their numerical approximation in the next section. This solution concepts allows for instance

topology changes of the evolving sets, which is especially for our application an important property. It is based on the theory of level set methods. In what follows, we close our model specifying suitable speed functions $F : \Omega \to \mathbb{R}_0^+$, which describe the front propagation. We suppose the speed function F to depend on local image properties and the shape of the local front. This approach is very flexible regarding the modeling of different homogeneity criteria, since arbitrary growing parameters can be very easily be considered to define combined speed functions. They should naturally be modeled in a way that they return high values for instance in areas of homogeneity and very small values in areas where a segment boundary is likely to be.

Suppose a boundary indicator function $\sigma : \Omega \to \mathbb{R}$ depending on the image intensity I is given. Then $\sigma(x) \geq 0$ indicates areas in which homogeneity is lost. Thus, we simply choose F to be the characteristic function $F := \chi_{\{\sigma<0\}}$, which would yield the desired segment $\mathcal{S}(\infty)$ (cf. [4]). As already discussed, it is locally not always clear how to construct a reliable and robust indicator. Thus we have to replace such a binary formulation. A suitable alternative is to give homogeneity a measure, here in terms of the speed. Hence in areas where the segment seems to stop, the propagation speed should decrease drastically. A straightforward modification of the above speed function would be to convolute σ in advance with a smooth kernel, but necessary information may lost.

Fig. 1. From left to right: original, gradient based speed, gray value based speed, min-combination

Let us now list some more sophisticated possible choices for F:

- Analogously to a segmentation related to a range of gray-values we set $F_I := e^{-\frac{(I-\mu)^2}{2\sigma^2}}$ with a maximum of 1 at a given "best" reference gray value μ. Deviations $|I(x) - \mu|$ are penalized by a decrease of F_I. The parameter σ controls the sensitivity of F_I to this deviation.
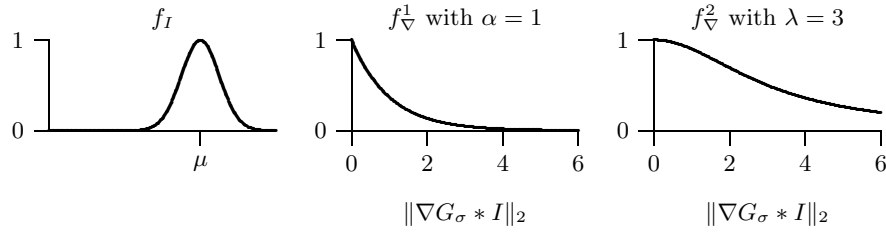
Fig. 2. The different gray value and gradient dependant speed functions.

- For larger gray value intervals $[\varrho_-, \varrho_+]$ we consider a convolution of the corresponding characteristic function $\chi_{[\varrho_-,\varrho_+]}$ by some Gaussian kernel G_σ of width σ, i.e. we choose $F_I := G_\sigma * \chi_{[\varrho_-,\varrho_+]}$.

- Another well known segmentation method depicts large gradients to define edges and segment boundaries respectively. Instead of a fixed threshold for the gradient magnitude we again construct a F which decreases substantially in areas of large gradients. Possible choices are $F_\nabla^1 := e^{-\alpha\|\nabla G_\sigma * I\|}$ and $F_\nabla^2 := \frac{1}{1 + \frac{\|\nabla G_\sigma * I\|_2^2}{\lambda^2}}$, where the parameters α, λ strengthen or weaken the build in edge indicator.

- In the evolution of interfaces under mean curvature [16] the speed function $F = -H$ is used, where H denotes the mean curvature $\nabla \cdot \left(\frac{\nabla \Phi}{|\nabla \Phi|} \right)$ We incorporate this term into our speed function $\tilde{f} := \max(f - \epsilon \max(H, 0), 0)$ for sufficiently small ϵ. This results in a deceleration of the evolution in regions, where the curvature of the interface is positive and large, preventing the growing into other regions which are reachable only via small and narrow bands.

- In more complex and subtle applications it is in general appropriate to consider algebraic combinations of the latter indicators, e. g. $F_1 \cdot F_2$, $\min(F_1, F_2)$, $\max(F_1, F_2)$.

- Often certain segments have already been extracted from the image, which are known not to intersect with the segment under consideration. If we denote the union of these sets B, we can modulate a given speed function F corresponding choosing $F(1 - \chi_B)$, where χ_B is the characteristic function of B. Examples in tissue segmentation are bones, vessels an other tissue types.

In the application flexibility in the selection of criteria and the choice of parameters is the key for a fast and successful automatic or at least semiautomatic segmentation.

4 An adaptive algorithm based on hexahedral and quadrilateral multilevel grids
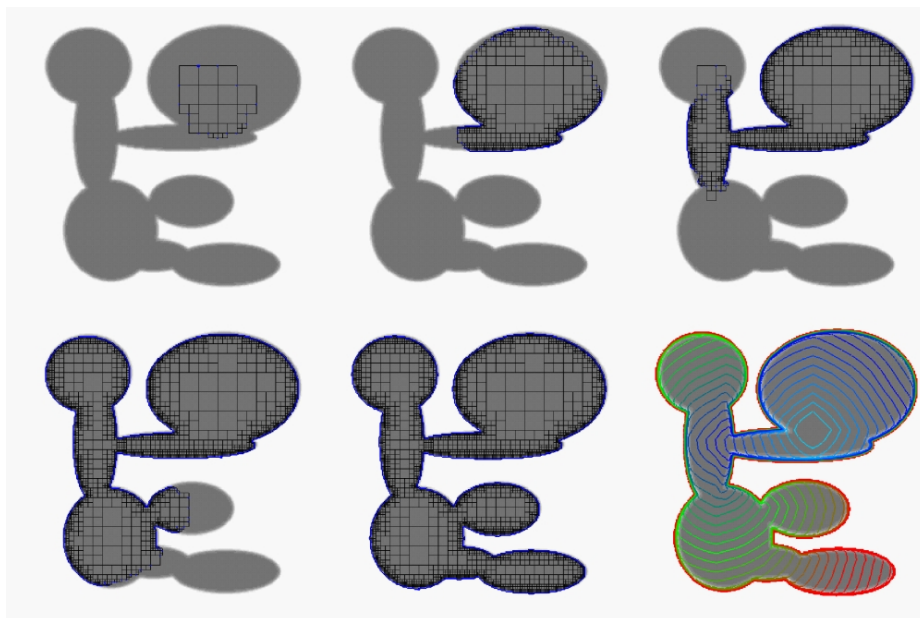

Fig. 3. The adaptive grid grows along with the computation of new nodes. On the bottom right different isolines of the solution are depicted.

One of the main contributions of this paper is the computational speedup of the fast marching method [18] by using an adaptively generated grid. Different from previous work this grid is implicitly described by error indicator values η on elements. Due to a given threshold value ϵ we locally stay on fine grid cells or we confine with much coarser elements. As grids we consider in 2D quadrilateral and in 3D hexahedral meshes. Our finest level grid corresponds to the pixels or voxels of the original image. On top of this finest grid we build a hierarchical grid, i.e. a quadtree or an octree respectively.

At least the original grid can be embedded in some regular $(2^l_{\max})^d$ grid, e.g. by filling the superficious cells with some background intensity. Instead of some process solely on the finest grid level which successively visits all fine grid cells inside the segment, our aim is to compute the front propagation on coarse elements in the hierarchy of nested grids whenever possible.

Let us denote by $\mathcal{M} := \{\mathcal{M}^l\}_{l=1,\ldots,l_{\max}}$ the family of nested grids, each consisting of elements or cells E and nodes $\mathcal{N}(\mathcal{M})$ such that $\bigcup_{E \in \mathcal{M}^l} E = \Omega$ for all $l = 1, \ldots, l_{max}$. They are supposed to be nested in the sense that for all $E^{l+1} \in \mathcal{M}^{l+1}$ there exists an $E^l \in \mathcal{M}^l$ such that $E^{l+1} \subset E^l$. Furthermore, let us suppose that an error function $\eta^*(\cdot)$ is given as function a $\eta^* : \Omega \to \mathbb{R}$ on the image depending on the image intensity or some derived quantity. We can locally evaluate this function at the centers of elements E on the finest grid and obtain our initial error indicators on finest grid cells. Next, we have to define error indicator values on the coarser parent element in the tree structure.

To ensure that our grid hierarchy has only one–level transitions between neighboring cells - which turns out to be preferable concerning the algorithm - we require the following properties:

$$\eta(E) \leq \eta(\mathcal{P}(E)) \text{ for all } E \in \mathcal{M} \tag{2}$$
$$\eta(E) \leq \eta(\mathcal{P}(\tilde{E})) \text{ for all } \tilde{E} \in \mathrm{adj}(E) \tag{3}$$

Here $\mathcal{P}(E)$ denotes the unique parent element of E in the grid hierarchy, $\mathcal{C}(E)$ the set of children of E and $\mathrm{adj}(E)$ are the neighbouring elements of E on the same hierarchical level. Later we will use $\mathrm{adj}(N)$ where $N \in \mathcal{N}(\mathcal{M})$, as the set of all regular nodes connected to N by an edge. Observe that the inequality (3) ensures the one–level transitions between grid cells, whereas the saturation condition (2) guarantees that the error indicator on coarse cells indicate details on much finer cell. We ensure this property in a preroll step running the following algorithm.

Algorithm: Preroll estimator saturation

```
for each E ∈ M^l_max do η(E) := η*(c_E)
 for l = l_max-1 to 0 step -1 do
   for each element E of M^l do
```

$$\mathcal{A} \ := \ \mathcal{C}(E) \cup \texttt{adj}(\mathcal{C}(E))$$
$$\eta(E) \ := \ \texttt{max} \ (\eta(E), \texttt{max}_{\tilde{E} \in \mathcal{A}} \eta(\tilde{E}))$$

Here c_E is the center of mass of the element E. Let us emphasize that the level wise processing of elements from the finest up to the coarsest level is essential to ensure properties (2, 3). A simple depth first traversal of the tree structure doesn't achieve this goal.

Starting with the finest grid $\mathcal{M}^{l_{\max}}$ we can now recursively coarsen elements $E \in \mathcal{M}^{l_{\max}}$ by checking the indicator $\eta(E) < 0$ for each element. The result is an adaptive grid, which resembles the smoothness properties of the underlying mesh. As a simple choice for the error indicator function we choose the gradient of the image intensity

$$\eta^*(x) = \|\nabla I(x)\|_2.$$

Concerning the actual front propagation algorithm we consider a modification of the fast marching method presented in [1]. We denote by T_{ij} nodal values approximating the true propagation time T at a grid node x_{ij} and by F_{ij} the speed of propagation. Such a node x_{ij} appears on some grid level l for the first time. In what follows we either indicate it by x_{ij} or by x^l. Initially we suppose all T values on the nodes except those on the seed points to be set to ∞. Given all $F_{ij} > 0$ let us now review the following 2D upwind-scheme [18] – in the following the algorithm is described for simplicity in the 2D case, the 3D algorithm is formulated entirely analogous - for the generalized eikonal equation (1)

$$\max(D_{i-\frac{1}{2},j}T, -D_{i+\frac{1}{2},j}T, 0)^2 +$$
$$\max(D_{i,j-\frac{1}{2}}T, -D_{i,j+\frac{1}{2}}T, 0)^2 = \frac{1}{F_{ij}^2} \qquad (4)$$

We define $D_{i,j-\frac{1}{2}}T := h^{-1}(T_{ij} - T_{i-1,j}), D_{i,j+\frac{1}{2}}T := h^{-1}(T_{i+1,j} - T_{i,j})$ etc., where h denotes the gridsize. As described in detail in [18] the upwind-character of this scheme and the positivity allows the equation to be solved in a single expanding traversal of the grid nodes using for each node only upwind-values. The resulting algorithm is entirely nodal based. Once all the arrival times $T(x^l)$ at the nodes $x^l \in \mathcal{N}(E^l)$ are known for a given element $E^l \in \mathcal{M}^l$, all other values can be computed by bi- or trilinear interpolation.

Denote by $\mathcal{K}$ the set of *known* nodes of $\mathcal{M}$, i.e. the set of already computed nodes on the grid, $\mathcal{T}$ the set of *trial* nodes of $\mathcal{M}$ along the boundary of the area of computed values, $\mathcal{D}$ the set of *downwind* side nodes of $\mathcal{M}$, i.e. nodes with unknown arrival time values. We now have to make some modifications to the standard fast marching algorithm in order to implement adaptivity. Once the node N with minimal time is extracted from $\mathcal{T}$ and made active, all neighboring nodes regarding the adaptive grid have to be found. The values of these are updated if they are in $\mathcal{T}$ by solving the corresponding quadratic equation (4) using as many contributing known values as possible. Here we exploit the fact that our saturation generates only one–level transitions between neighboring grid cells. The appearance of hanging nodes can not be avoided in hexahedral and quadrilateral grids. The time values at hanging nodes will be computed by interpolation of all other known time values at the corresponding edge/face, hence we have to make sure that no hanging nodes will be added to $\mathcal{T}$. For each newly accepted node in $\mathcal{K}$ we have to check if there is a hanging node in the vicinity and interpolate it, if all other arrival times of the edge/face are known as well. In this way we have constructed an algorithm, which by only local operation generates a fully computed grid in the inside of the segment. Cells are marked and checked on the fly during the process of determining new trial nodes along the current computation boundary. If we have a bounding area $\mathcal{B}$ which surely contains the object of interest, we can stop the computation when all nodal values for the propagation time T are known in $\mathcal{B}$. Now we can formulate the

Algorithm: Adaptive Fast Marching Method

```
while ( T ≠ ∅ ) {
  take smallest N with minimal time out of T
  T = T \ {N} and K = K ∪ {N}
  for all Ñ ∈ adj(N) ∩ Kᶜ do {
    if Ñ is no hanging node and Ñ ∈ B {
      compute time value of Ñ according to (4)
      if the Ñ is on a face/edge with a hanging node and
        all time values on this face/edge are known {
        interpolate the hanging node }
```

$$\mathcal{T} = \mathcal{T} \cup \{\tilde{N}\} \ \} \ \} \ \}$$

Here $\mathcal{K}^c$ denotes the complement set of $\mathcal{K}$.
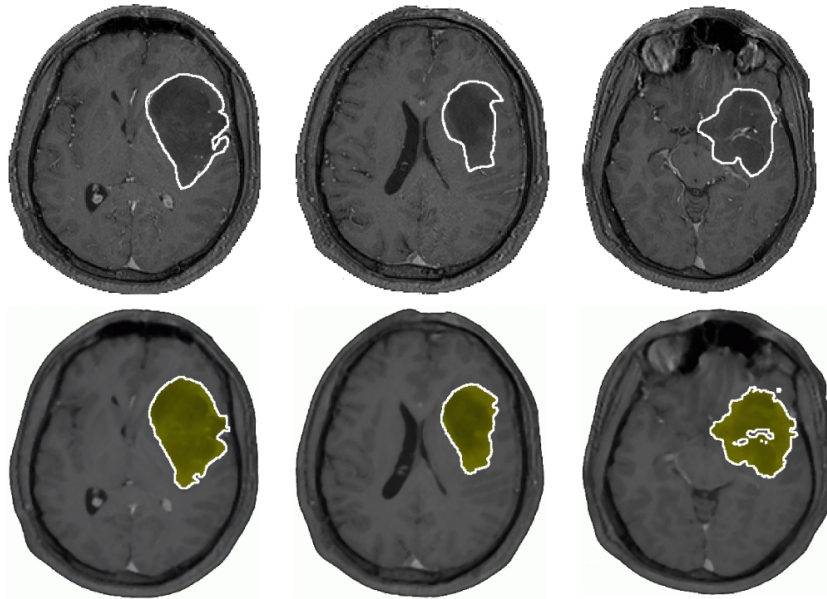
5 Application to medical data exploration

Fig. 4. Top: gliom boundary as evaluated from an experienced neurosurgeon. **Bottom**: slices through the 3D segmentation result for comparison

We will now describe how this method actually comes into play for a precise interactive segmentation process. The corresponding task - the extraction of glioma in 3D MRI data sets - has already been outlined in the introduction. Before the automatic segmentation by front propagation takes place the user only has to control a few functional parameters with an intuitive meaning. The gray value range can be determined by simply choosing a few characteristic points in the interior of the segment corresponding to a gray value. As shown in figure 3 the user gets an instant visual feedback of the speed function onto the original data slices, which allows a careful choice

of the adjustable parameters. The gradient parameters λ or α seldomly have to be changed and can be given a standard experience based value. These parameters can as well be used for the adaptive grid generation, which may be also based on the gray value interval of interest and a gradient magnitude threshold. As sometimes the speed function naturally has to respond to small variations of local homogeneity and MRI imaging is due to background noise, some anisotropic diffusion based prefiltering [21] significantly helps to prevent the creation of small noise–like artefacts on the surface.

We use complement segmentation as another auxiliary method to eventually avoid growth into areas of which we are sure to belong to the segments complement and are easy and efficiently to segment by the discrete multilevel segmentation method in [4]. We artificially let the combined speed F tend nearly to zero in these areas, which has shown to be helpful in some difficult cases.

After the computation of T is done around the segment, we have a whole family of isosurfaces $\partial \mathcal{S}(t)$ at hand. The clinician is only left to manually choose the desired isosurface by selecting a suitable parameter T. Hence, the corresponding 3D tumor segments or slices of it are visualized together with arbitrary slices of the original data set. Then the clinician interactively navigates through the family of tumors and selects a proper value T which best corresponds to his expertise knowledge. To test our adaptive front propagation segmentation method, we have compared its semi automatic segmentation mode in type 5a and 5b insular gliomas with the slice-by-slice demarcation method as performed by experienced neurosurgeons. As can be seen in figure 4 the segmentation results are very close to manual evaluation by perception even in the extremely ambiguous areas at the border of the tumor, where only marginal differences in image intensities are crucial. Due to adaptivity we have a finely resolved solution along the boundaries of the object.

The 3D segmentation based on our algorithm requires about 30 sec including the required user interaction. The actual computation of the front propagation takes about 5 seconds for the identification of glioma as depicted in the figures throughout the paper. Compared to this a manual segmentation on each slice by an experienced neurosurgeon takes at least half an hour concentrated work.
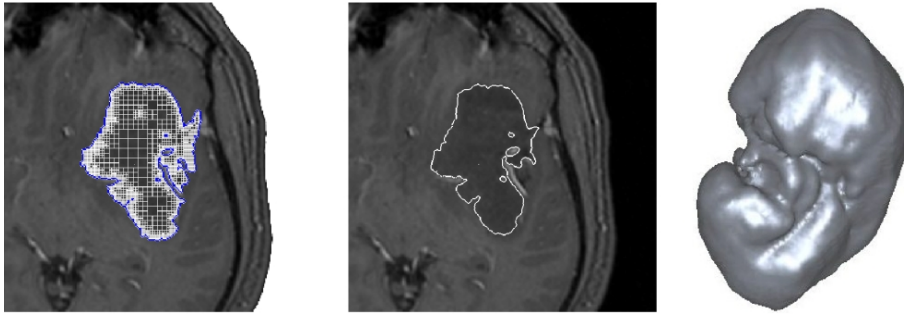
Fig. 5. Left: a slice through the generated 3D-grid. **Middle**: The curvature criterion will prevent the small structure on the right to leak out. **Right**: The final rendered isosurface.

6 Conclusions

We have presented a multilevel front propagation algorithm for segmentation purposes on medical images. It is based on the nowadays widespread level set techniques and allows the robust and flexible segmentation of regions with non sharp boundaries with only very limited and intuitive user interaction. As an application we have considered the extraction of glioma regions in the human brain. The peculiarities of the presented method are the variety of criteria which are considered to flexibly model the speed of propagation, especially including curvature terms which avoid fingering artifacts on the front, and the underlying adaptive grid concepts responsible for the nearly real time performance of the algorithm. Thereby, our adaptive method handles grids solely procedurally without storing graphs for the underlying hierarchical grids. We confine with error indicator values on the nodes of the image discretization to steer the grid traversal appropriately. A saturation condition ensures sufficient regularity of the grid. Some future research direction are

- the investigation on different, local filters which lead to additional indicators for segment boundaries,
- the collection of a library of speed functions well suited for the segmentation of different types of tumors and other tissue types,
- and the improvement of the currently experimental user interface.

References

1. D. Adalsteinsson, R. Kimmel, R. Malladi, and J. A. Sethian. Fast marching methods for computing the solutions to static hamilton-jacobi equations. *CPAM Report 667, University of Berkeley*, 1996.

2. V. Caselles, F. Catté, T. Coll, and F. Dibos. A geometric model for active contours in image processing. *Numer. Math.*, 66, 1993.

3. M. G. Crandall and P. L. Lions. Viscosity solutions of hamilton-jacobi equations. *Tran. AMS, 277*, pages pp. 1–43, 1983.

4. M. Droske, T. Preußer, and M. Rumpf. A multilevel segmentation method. In *proceedings of VMV, Max Planck Institut für Informatik, Saarbrücken*, 2000.

5. H. Duffau, L. Capelle, M. Lopes, T. Faillot, J. P. Sichez, and D. Fohanno. The insular lobe: Physiopathological and surgical considerations. *Neurosurgery 47*, pages pp. 801–811, 2000.

6. J. M. Gauch. Image segmentation and analysis via multiscale gradient watershed hierarchies. *IEEE Transactions on Image Processing*, 8(1), 1999.

7. D. Geman, S. Geman, C. Graffigne, and P. Dong. Boundary detection by constrained optimization. *IEEE Transactions on Pattern Analysis and Machine Intelligence*, pages 609–628, 1990.

8. K. Haris, S. N. Efstratiadis, N. Maglaveras, and A. K. Katsaggelos. Hybrid image segmentation using watersheds and fast region merging. *IEEE Transactions on Image Processing*, 7(12), 1998.

9. G. A. Hewer, C. Kenney, and B. S. Manjunathg. Variational image segmentation using boundary functions. *IEEE Transactions on Image Processing*, 7(9), 1998.

10. T. Kapur, W. Grimsol, W. WellsIII, and R. Kikinis. Segmentation of brain tissue from magnetic resonance image. *Medical Image Analysis*, 1(2), 1997.

11. R. Malladi and J. A. Sethian. Level set methods for curvature flow, image enhancement and shape recovery in medical images. In *Proc. of Conf. on Visualization and Mathematics, June, 1995, Berlin, Germany*. Springer-Verlag, Heidelberg, Germany, 1997.

12. R. Malladi, J. A. Sethian, and B. C. Vemuri. Shape modelling with front propagation. *IEEE Trans. Pattern Anal. Machine Intell.*, 17, 1995.

13. F. Meyer and S. Beucher. Morphological segmentation. *J. Vis. Commun. Image Represent.*, 1:21–46, 1990.

14. B. Milne. *Adaptive Level Set Methods Interfaces*. PhD thesis, PhD. Thesis, Department of Mathematics, University of California, Berkeley, CA., 1995.

15. D. Mumford and J. Shah. Boundary detection by minimizing functionals. pages 22–26, 1985.

16. S. Osher and J. A. Sethian. Fronts propagating with curvature–dependent speed: Algorithms based on hamilton–jacobi formulations. *J. Comput. Phys., Vol. 79*, pages 12–49, 1988.

17. Y. Sato, S. Nakajima, N. Shiraga, H. Atsumi, S. Yoshida, T. Koller, G. Gerig, and R. Kikinis. Three-dimensional multi-scale line filter for segmentation and visualization of curvilinear structures in medical images. *Medical Image Analysis*, 2(2), 1998.

18. J. A. Sethian. *Level Set Methods and Fast Marching Methods*. Cambridge University Press, 1999.

19. K. Siddiqi, Y. B. Lauzière, A. Tannenbaum, and S. W. Zucker. Area and length minimizing flows for shape segmentatio. *IEEE Transactions on Image Processing*, 7(3), 1998.

20. L. Vincent and P. Soille. Watersheds in digital spaces: An efficient algorithm based on immersion simulations. *IEEE Trans. Pattern Anal. Machine Intell.*, 13, 1991.

21. J. Weickert. *Anisotropic Diffusion in Image Processing*. Springer, 1998.

22. C. Xu and J. L. Prince. Snakes, shapes, and gradient vector flow. *IEEE Transactions on Image Processing*, 7(3), 1998.

23. M. G. Yasargil, K. von Ammon, E. Cavazos, T. Doczi, J. D. Reeves, and P. Roth. Tumours of the limbic and paralimvic systems. *Acta Neurochir 118*, pages pp. 40–52, 1992.

24. J. Zentner, B. Meyer, A. Stangl, and J. Schramm. Intrinsic tumors of the insula: A prospective surgical study of 30 patients. *Neurosurgery 85*, pages pp.263–271, 1996.